Journal of Photochemistry and Photobiology A: Chemistry 208 (2009) 203–212

Contents lists available at ScienceDirect

Journal of Photochemistry and Photobiology A: Chemistry

journal homepage: www.elsevier.com/locate/jphotochem

Long-lived electron–hole pair formation through photoionization of diphenylacetylene occluded in medium pores of aluminum rich $M_{6.6}$ZSM-5 zeolite ($M = Li^+$, Na^+, K^+, Rb^+, Cs^+) Influence of the counterbalancing cations on the recombination rate

F. Belhadj [1], A. Moissette *, C. Brémard

Laboratoire de Spectrochimie Infrarouge et Raman, UMR-CNRS 8516, Centre d'Etudes et de Recherches Lasers et Applications, FR-CNRS 2416, Bât. C5 Université des Sciences et Technologies de Lille I, 59655 Villeneuve d'Ascq Cedex, France

ARTICLE INFO

Article history:
Received 1 July 2009
Received in revised form 8 September 2009
Accepted 16 September 2009
Available online 23 September 2009

Keywords:
ZSM-5
Diphenylacetylene
Charge separation
Photoionization
Diffuse reflectance UV–vis spectrometry
Kinetic

ABSTRACT

Diffuse reflectance UV–vis and Raman spectroscopies show complete sorption of neutral diphenylacetylene (DPA) in the void space of $M_{6.6}$ZSM-5 zeolites ($M = Li^+$, Na^+, K^+, Rb^+, Cs^+) after several months of exposure of solid DPA to empty zeolite at room temperature. After a long organization period, the laser photolysis of DPA occluded in $M_{6.6}$ZSM-5 generates long-lived $DPA^{\bullet+}$ radical cation as primary phenomenon. Charge recombination occurs mainly through electron transfer and DPA@$M_{6.6}$ZSM-$5^{\bullet-\bullet+}$ electron–hole pair formation. This subsequent electron transfer takes place between the electron deficient radical cation $DPA^{\bullet+}$ and the electron donor oxygen atom of zeolite framework. The multivariate curve resolution analysis of the DRUVv spectra recorded during the reaction sequence including charge separation, electron transfer and charge recombination provide the specific absorption spectra and respective spectral concentrations of all species as function of time. The DRUVv spectrum assigned to the long-lived DPA@$M_{6.6}$ZSM-$5^{\bullet-\bullet+}$ electron–hole pair exhibits broad bands between 450 and 550 nm. The electron–hole pair recombination depends on M^+ and appears to be in relation with the electron donor properties of the framework. The charge recombination rate decreases in the order $Cs^+ > Rb^+ \sim K^+ > Na^+ > Li^+$. The electron–hole pair lifetime exceeds several hours at room temperature. The stabilization of $DPA^{\bullet+}$-electron pair and DPA@$M_{6.6}$ZSM-$5^{\bullet-\bullet+}$ electron–hole pair depends on the combined effects of confinement which dramatically reduces the DPA mobility in the zeolite void space and on the intrazeolithe electrostatic field of DPA@M_nZSM-5 ($M = Li^+$, Na^+, K^+, Rb^+, Cs^+).

1. Introduction

Diphenylacetylene (DPA) is a molecule of primary importance because it represents the structural unit of the phenylene acetylene oligomers that are involved in many applications. Because of their good rigidity and conductivity, DPA derivatives constitute a wide range of compounds that present a great potential for many applications in the field of molecular electronic devices. DPA can be used as a model to investigate and to understand the electron and charge transfers in all DPA based oligomers. They can act as molecular switches [1], molecular memory devices [2,3] and digital computers [4]. Some DPA oligomers are also considered as ideal prototypes for molecular wires [5] and can be incorporated into liquid crystalline compounds also to improve the optical behavior of the materials [6].

The development of macromolecular systems that are capable of generating a long-lived generated state is of particular interest for technological advances in solar energy conversion and molecular devices. In simple molecular dyads that demonstrate rapid rates of charge separation, the efficient generation of the photocurrent has not been yet achieved because of too fast charge recombination after photoirradiation [7,8]. Therefore, to generate a long-lived charge separated state, the charge recombination must be slowed down by spatially separating positive and negative charges. As predicted from the electron transfer theory, the rates of charge recombination between the electron donor and acceptor are dependent upon the energetics and in particularly of the driving forces of the process [9]. In this context, the dynamics of charge separation and charge recombination in synthetic DNA hairpins in which DPA organic chromophores are used as linkers have been investigated [10,11]. Hence, the core function of the reaction is a sequence of photoinduced energy and electron transfers between donors and

* Corresponding author.
E-mail address: alain.moissette@univ-lille1.fr (A. Moissette).
[1] Present address: Laboratoire de Chimie Physique, Université des Sciences et de la Technologie Mohamed Boudiaf USTO - BP 1505 El Mnaouer, Oran, Algeria.

1010-6030/$ – see front matter © 2009 Elsevier B.V. All rights reserved.
doi:10.1016/j.jphotochem.2009.09.016

acceptors in the antenna complexes and the reaction center. Among various systems nanoporous aluminosilicate materials like zeolites are of particular importance for the construction of models. They constitute organized host guest systems materials in which the host imposes a specific spatial organization to selected active molecules and because of high polarization and high confinement effect, such environment might induce spontaneous ionization of low ionization potential molecules. Zeolites have shown high potential for stabilizing charge separation states spontaneously created or photoinduced [12–21].

Among zeolites, ZSM-5 are crystalline aluminosilicates possessing an open framework of molecular-sized straight and zigzag channels. Rod-shape molecules like polyaromatic hydrocarbon or diphenyl polyene were reported to enter through the straight channels and to exhibit close match with the pore size [22–26]. Due to the presence of trivalent aluminum in the framework, the net charge of aluminum is negative and must be counterbalanced by a cation. Nevertheless, the M^+ cations do not only act as simple charge compensating species but also affect drastically the electron donor strength of the zeolite framework and therefore the stabilization of charge separated states. The double role of electron acceptor and electron donor of the zeolite framework was already observed as well after sorption and subsequent photoionization of rod-shaped molecules as after spontaneous ionization [27–31]. Furthermore, it was established previously not only within narrow pore ZSM-5 [32–35] but also within the larger cavity Y zeolite [18] that the nature of the extra framework cation affects significantly the distance of electron migration within the framework and therefore the lifetime of charge separated states. Consequently, according to zeolite properties and because DPA stands for the structural unit of the conjugated oligomers and can provide a good model for investigating the structural and electronic properties that control the electron transport in phenylene acetylene oligomers, in the present work we seek to study the effect of the zeolite void space on charge separated state created by photoexcitation of previously occluded DPA. First, we employ diffuse reflectance UV–vis absorption (DRUVv) and Raman scattering spectroscopies to monitor the course of DPA sorption in aluminum rich $M_{6.6}$ZSM-5 zeolites for various alkali extraframework cations ($M = Li^+$, Na^+, K^+, Rb^+, Cs^+), under dry and inert atmosphere without any solvent. The conformations and sorption sites of occluded DPA are predicted using Monte Carlo simulations and subsequent molecular mechanics calculations. This modeling study is expected to support the structural interpretation of the spectroscopic results. After laser photolysis, the fate of the photoinduced $DPA^{\bullet+}$-electron pair is explored over several days. Multivariate chemometric methods are used to resolve the UV–vis absorption spectra and spectral concentrations of pure species involved in the ionization, electron transfer and charge recombination course. The lifetimes of $DPA^{\bullet+}$-electron moiety and subsequent electron–hole pair are obtained by data processing.

2. Experimental

2.1. Materials

As-synthesized $Na_{6.6}$ZSM-5 samples (Si/Al = 13.5, average particle size 1 μm) were obtained according to the template procedure in alkaline medium from VAW aluminum (Schwandorf, Germany). Crystals of silicalite-1 (Si/Al > 1000, average particle size 2 μm) were synthesized in high purity according to the fluoride medium procedure in the "Laboratoire des Matériaux à Porosité Contrôlée", UMR-CNRS 7016, Mulhouse, France. The as-synthesized ZSM-5 zeolites were calcined under air to evacuate the template. The extra framework cations were completely exchanged by Li^+, K^+, Rb^+, Cs^+. The exchange was carried out according to the processes reported previously [36]. All the bare zeolite samples were dehydrated by a calcination procedure up to 773 K under argon. The chemical analyses, powder XRD patterns, ^{29}Si, ^{27}Al MAS-NMR, IR, Raman, DRUVv, and EPR spectra of $Na_{6.6}$ZSM-5 sample were found to be characteristic of well-crystallized porous compound with following formulae per unit cell: $M_{6.6}(AlO_2)_{6.6}(SiO_2)_{89.4}$. Particularly, no evidence was found for Brønsted acidic sites using IR absorption spectrometry and pyridine absorption.

Diphenylacetylene (DPA 99% $C_{14}H_{10}$, ACROS Organics) was purified by sublimation and stocked over molecular sieves. Pure and dry Ar gas was used.

2.2. DPA sorption in M_nZSM-5

Weighed amounts (~1.4 g) of powdered hydrated zeolite $M_n(AlO_2)_n(SiO_2)_{96-n}$ were introduced into an evacuable heatable silica cell. The sample was heated up to 773 K under Ar. Then, the sample was cooled to room temperature under dry argon. Weighed amounts of DPA corresponding to 1 DPA/UC were introduced into the cell under dry argon and the powder mixture was shaken. The powders were transferred under dry argon in a quartz glass Suprasil cell for Raman and DRUVv experiments. The powder mixtures were left at room temperature. The loaded $DPA@M_{6.6}(AlO_2)_{6.6}(SiO_2)_{89.4}$ samples were studied and irradiated after complete sorption and equilibration.

2.3. Molecular modeling

The molecular modeling of the DPA preferred sorption sites in $M_n(AlO_2)_n(SiO_2)_{96-n}$ zeolites was performed using Material Studio Modeling package (version 4.4) from *Accelrys International*. The structural parameters and partial atomic charges of silicalite-1 with $(SiO_2)_{96}$ unit cell were taken from previous work [37]. The M_6ZSM-5 structural model was built from the location of Al framework atoms deduced from the Cs^+ location in several series of Cs-exchanged MFI phases determined at several Si/Al ratios [38–42]. The structural parameters and set of partial atomic charges of DPA were derived from previous structural and theoretical works [43–45]. The non-bonding Lennard–Jones (L–J) force field values were taken from previous works [37,46]. The simulation box consists of $2 \times 2 \times 4$ orthorhombic cells. In the Monte Carlo (MC) calculations, the Si, Al, O and M^+ ($M = Li^+$, Na^+, K^+, Rb^+, Cs^+) positions were fixed in the simulation box. Periodic boundary conditions were applied in all directions. The DPA structure was taken to be rigid.

The MC simulations at 1 DPA/UC loading were carried out at 300 K using the conventional Metropolis algorithm taking into account the non-bonding interactions (E_{ZS}) between the O and M^+ atoms of zeolite and the C and H atoms of DPA as well as the non-bonding interactions (E_{SS}) between DPA. The interactions inside the zeolite were modeled by L–J and coulombic forces.

$$E_{ZS} + E_{SS} = \frac{A_{\alpha\beta}}{r_{ij}^{12}} - \frac{B_{\alpha\beta}}{r_{ij}^{6}} + \frac{q_i q_j}{r_{ij}} \quad (1)$$

A cut-off radius of 0.9 nm was applied to the L–J interactions. The long-range electrostatic interactions were calculated using the Ewald summation method. The simulation takes a number of steps to equilibrate from its original random position. From each sorption trajectory, a histogram of the energy distribution for sorbate was generated. In a so-called mass-cloud analysis the center of mass of DPA in each configuration was displayed as a dot in the model space. In the molecular mechanics (MM) simulations the time consuming Ewald summation has not been used. The zeolite framework was taken to be fixed and the M^+ extraframework cations and DPA

were taken to be mobile. The energy minimization of non-bonding sorbate-zeolite energy was performed using the conjugate gradient minimization procedure.

2.4. Photolysis

The photolysis of the bare $M_n(AlO_2)_n(SiO_2)_{96-n}$ and loaded DPA@$M_n(AlO_2)_n(SiO_2)_{96-n}$ (n = 0, 6.6) samples were carried out at room temperature during 15 s with a pulsed Nd:YAG laser (20 ns, 20 Hz) operating at 266 nm wavelength with 60 mW/cm^2 power. The 266 nm wavelength is resonant with the electronic transitions of occluded DPA.

The UV–vis diffuse reflectance and Raman spectra were recorded at room temperature before and after the laser irradiation period as a function of time over several days.

2.5. Instrumentation

2.5.1. Diffuse reflectance UV–vis absorption (DRUVv)

The UV–vis absorption spectra of the powdered samples were recorded between 200 and 900 nm using Cary 3 spectrometer. The instrument was equipped with an integrating sphere to study the powdered zeolite samples through diffuse reflectance; the corresponding bare zeolite was used as the reference. The DRUVv spectra were plotted as the Kubelka–Munk function:

$$\boldsymbol{F}(R) = \frac{(1-R)^2}{2R} = \frac{K}{Sc} \quad (2)$$

where R represents the ratio of the diffuse reflectance of the loaded zeolite to that of the dehydrated neat zeolite, K designates an absorption coefficient proportional to the concentration C of the chromophore and Sc the scattering coefficient of the powder. Spectral sets $\boldsymbol{F}(\lambda, t)$ were recorded as function of λ (wavelength) at several t (time) during the course of the DPA sorption and after photoionization.

2.5.2. Raman scattering spectroscopy

A Bruker RFS 100/S instrument was used as a near-IR FT-Raman spectrometer with a CW Nd:YAG laser at 1064 nm as the excitation source. A laser power of 100–200 mW was used. The spectra (3500–150 cm^{-1}) were recorded with a resolution of 2 cm^{-1} using 600 scans.

The Raman spectra obtained by using the 785 nm exciting line were collected on a Kaiser spectrometer equipped with a Peltier-cooled charge-coupled device detector. The laser line was supplied by a laser diode.

A LabRAM spectrometer (Jobin Yvon Horiba Gr.) equipped with a liquid-nitrogen-cooled charge-coupled device detector was also used with an excitation at 632.8 nm in the visible spectral domain. The laser radiations were supplied by a helium–neon laser. A 50× Ultra Long Work Distance (Olympus ULWD) objective was used to excite and to collect the Raman scattering of the sample within the cell. The laser power delivered was 8 mW and could be monitored via a filter wheel with the optical densities 0.3, 0.6, 1, 2, 3, and 4.

2.6. Data processing

2.6.1. Multivariate curve resolution (MCR) data processing

The MCR data processing of DRUVv spectral set $\boldsymbol{F}(\lambda, t)$ was carried out by MCR processing using the SIMPLISMA (SIMPle-to-use Interactive Self-modeling Mixture Analysis) approach. This method was applied to extract pure DRUVv absorption and respective concentration (C) from spectral data recorded as a function of time after powder mixing without any prior information. $\boldsymbol{F}(\lambda, t)$ represents the original data matrix with spectra in rows. Primarily, it is necessary to estimate the global rank of $\boldsymbol{F}(\lambda, t)$ to estimate the number of pure absorbing species (k) present in the whole data set of the complex mixture. The $\boldsymbol{F}(\lambda, t)$ matrix is then decomposed into the following form:

$$\boldsymbol{F}(\lambda, t) = \boldsymbol{C_s}(t) x \boldsymbol{S_\lambda^T} + \boldsymbol{E} \quad (3)$$

$\boldsymbol{C_s}(t)$ represents the 'spectral concentration' matrix. $\boldsymbol{S_\lambda^T}$ represents the transpose of $\boldsymbol{S}_\lambda$ (spectral matrix) and $\boldsymbol{E}$ represents the residual error. The SIMPLISMA approach was applied to resolve both the concentration matrix $\boldsymbol{C_s}(t)$ (k columns and t rows) and the spectral matrix $\boldsymbol{S_\lambda^T}$ of pure compounds (k rows and λ columns $\boldsymbol{S_\lambda^T}$ and $\boldsymbol{C_s}(t)$ were calculated by standard matrix algebra according to the procedure detailed in the original publication without any prior information [47]. The difference between original and reconstructed data set lower than 5% *RRSSQ* (relative root of sum of square differences) provides a realistic picture of the components. The relative root of sum of square differences (*RRSSQ*) expresses the difference between the experimental data set $\boldsymbol{F}(\lambda, t)$ and the calculated data set $\boldsymbol{F}(\lambda, t)^{calc}$. The optimization is carried out using $\boldsymbol{C_s}$ and $\boldsymbol{S^T}$ initial estimates obtained by SIMPLISMA approach. Convergence is achieved when the standard deviation σ of residuals with respect to experimental data is less than 3%.

2.6.2. Kinetic calculations

The charge recombination kinetic was analyzed through the $C(t)$ decay. Mono or two exponentials do not reproduce accurately the decays. The concentration decay $C(t)$ was accurately fitted using the Albery function. The Albery function takes into account the non-homogeneity of the material [48]. According to the model, the time-dependent absorption profile of species can be represented by Eq. (4):

$$C(t) = \frac{\int_{-\infty}^{+\infty} \exp(-x^2)\exp(-\bar{k}t\exp(\gamma x))\,dx}{\int_{-\infty}^{+\infty} \exp(-x^2)\,dx} \quad (4)$$

where $\int_{-\infty}^{+\infty} \exp(-x^2)\,dx = \sqrt{\pi}$ and $C(t)$ is the normalized concentration, $\bar{k}$ is the average rate constant, and γ is the width of the distribution. If $\gamma = 0$ (no dispersion), Eq. (4) is reduced to a first order kinetics: $C(t) = \exp(-\bar{k}t)$. The decay kinetics fitting was carried out by using the Microcal™ Origin software.

3. Results

3.1. Sorption of DPA in M_nZSM-5 (M = Li$^+$, Na$^+$, K$^+$, Rb$^+$, Cs$^+$, n = 0, 6.6)

When a calculated quantity of solid yellowish DPA corresponding to 1 DPA per M_nZSM-5 unit cell (UC) (M = Li$^+$, Na$^+$, K$^+$, Rb$^+$, Cs$^+$, n = 0, 6.6) was exposed in the dark and under argon to dehydrated white zeolite powder, the powder remains white. The inter- and intra-crystalline migrations of DPA were monitored by conventional diffuse reflectance UV–vis absorption spectroscopy (DRUVv) and non-resonant FT-Raman spectroscopy.

The UV bands observed in the 250–350 nm wavelength regions for DPA powder dispersed in the M_nZSM-5 sample evolved slowly to intense absorption. The cation type did not induce significant spectral shift. The diffuse reflectance UV–vis absorption (DRUVv) indicates DPA complete sorption in M_nZSM-5 as intact molecule after several months at 300 K. The DRUVv absorption spectrum of occluded DPA exhibits a broad band with two maxima at 298 at 280 nm (Fig. 1).

The near-IR FT-Raman spectra recorded several months after mixing DPA and zeolite powders are presented in Fig. 2. The isolated DPA molecule in the S_0 state is known to be in a planar linear structure having D_{2h} molecular symmetry in the crystalline state. The main bands observed for solid DPA are assigned to the follow-

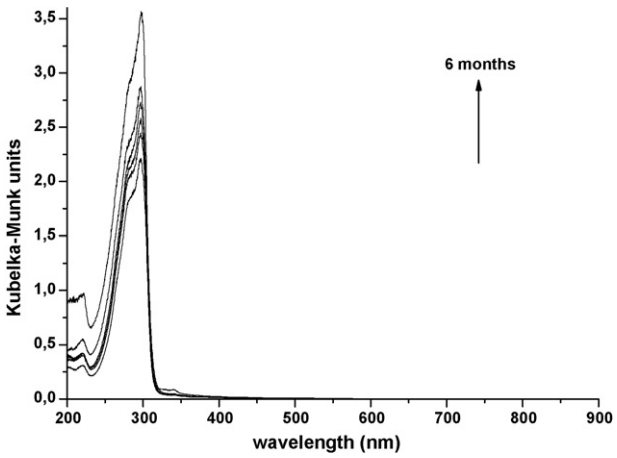

Fig. 1. Diffuse reflectance UV–vis absorption (DRUVv) spectra recorded for 6 months during DPA sorption into $Li_{6.6}$ZSM-5 zeolite. Solid DPA (1 DPA per UC loading) and $Li_{6.6}$ZSM-5 dehydrated under Ar at 773 K were mixed under Ar.

ing molecular modes: 384 (B_{2g}, medium), 538 (B_{2g}, m), 997 (A_g, strong), 1140 (A_g, s), 1483 (A_g, s), 1591 (A_g, very strong), 2219 (A_g, vs), 3052 (A_g, m) and 3064 cm^{-1} (A_g, m) [49,50]. After 2 months, the Raman spectrum of DPA occluded in silicalite-1 is very similar to that obtained in acetonitrile solution (Fig. 2b) [51]. In particular, the ring breathing and ring stretching are observed at 999 and at 1597 cm^{-1}, respectively, whereas the CH stretching are observed at 3062 and 3085 cm^{-1}. The most probable geometry in solutions is considered to be the same as that at the solid state [52]. These spectra are in agreement with D_{2h} molecular symmetry and the breakdown of the Raman selection rules does not occur despite the polarizable environment and the long organization period. The close match between the Raman features in solution and occluded in silicalite-1 demonstrate that the motions of DPA within the channels of this aluminum free zeolite are in the range of the isotropic limit of a liquid at room temperature. The most prominent Raman bands of zeolite are clearly observed around 800 and 380 cm^{-1} (not shown). Five months after mixing DPA and $M_{6.6}$ZSM-5 ($M = Li^+$, Na^+, K^+, Rb^+, Cs^+) the sorption induces also weak changes on DPA Raman bands which depend on the chemical composition of the zeolite host. The entrapment of DPA in $M_{6.6}$ZSM-5 ($M = Li^+$, Na^+) induces only very weak frequency shifts of the DPA Raman bands (Fig. 2, spectra c and d) and points out weak supplementary effect of the

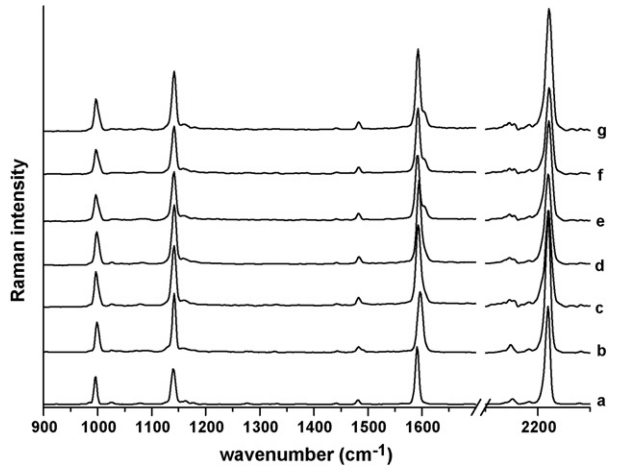

Fig. 2. Room temperature FT-Raman spectra (1064 nm laser exciting line) of DPA@M_nZSM-5 ($n = 0, 6.6$) recorded at room temperature several months after mixing of solid DPA and dehydrated M_nZSM-5: (a) solid DPA; (b) silicalite-1 ($n = 0$); (c) $Li_{6.6}$ZSM-5; (d) $Na_{6.6}$ZSM-5; (e) $K_{6.6}$ZSM-5; (f) $Rb_{6.6}$ZSM-5; (g) $Cs_{6.6}$ZSM-5.

electrostatic field. The entrapment of DPA in the pores of $M_{6.6}$ZSM-5 exchanged with bulky $M^+ = K^+$, Rb^+ and Cs^+ induces more marked spectral changes. Especially for these cations, a supplementary band is clearly observed at 1605 cm^{-1} as a shoulder of the band corresponding to the ring stretching mode centered at 1594 cm^{-1} (Fig. 2, spectra d–f). The ring breathing observed at 997 cm^{-1} shows also another weaker contribution at 1003 cm^{-1}. These new bands arise probably from weak structural changes induced by lowering of the local symmetry. The lower local symmetry promotes the breakdown of the Raman scattering selection rules of the free DPA molecule (D_{2h}). The new Raman bands are probably induced by combined effects of confinement and electrostatic field in the sorption site.

DRUVv and FT-Raman spectra recorded during the course of the DPA sorption in non-Brønsted acidic M_nZSM-5 zeolites indicate that complete sorption takes place according to Eq. (5) for $n = 0.0$, 6.6 and $M = Li^+$, Na^+, K^+, Rb^+, Cs^+.

$$DPA + M_nZSM\text{-}5 \rightarrow DPA@M_nZSM\text{-}5 \quad (5)$$

It is worth noting that the mere mixing of DPA with acid HZSM-5 induced DPA spontaneous ionization. The corresponding data fall beyond the scope of this study and are not presented here.

3.2. Molecular modeling of DPA occluded in M_nZSM-5

The framework structure of bare M_nZSM-5 zeolites and silicalite-1 contains two types of intersecting channels [53–55]. Both are formed by rings of 10 oxygen atoms, characterizing them as a medium-pore zeolite. One channel type is straight and has a nearly circular opening (0.53 nm × 0.56 nm), while the other one is sinusoidal and has an elliptical opening (0.51 nm × 0.55 nm). The predictions of the energy and structure of DPA sorption site in silicalite-1 host were carried out at 300 K and at constant loading (1 DPA/UC) by Monte Carlo (MC) simulations using the conventional Metropolis algorithm. The calculations took into account the non-bonded interactions between the fixed structure of silicalite-1 and rigid DPA. The energy distribution of individual DPA exhibits one broad maximum in silicalite-1. The corresponding distributions of the positions occupied by the DPA center of mass indicate that the net potential surface accessible to the molecule is maximum in the straight channel in the vicinity of the intersection with the zigzag channel. The energy minimization procedure taking DPA as mobile demonstrates that DPA undergoes only very weak influence of zeolite and remains in the range of the isotropic limit of a liquid at room temperature.

For M_nZSM-5 with aluminum content, currently no direct experimental information of the Al atom location is available. As used recently for modeling purpose, we explicitly distinguish silicon from aluminum sites with partial and random occupation according to the aluminum content [37]. Because of the strong coulombic interactions with the zeolite framework, the energetically most favorable positions for the M^+ cations are near the O atoms binding Al atoms. The energy minimization procedure taking DPA and extra framework cation as mobile leads to the structural situation presented in Fig. 3 for Na^+. DPA is occluded in the straight channel at the intersection of the straight and sinusoidal channels along the *b* axis. The energy minimization predicts a DPA quasi planar conformation. Only weak rotation of the phenyl groups about the C≡C triple bond is observed. Possible rotation is in agreement with the low torsion barrier previously reported in the literature [56–58]. The interaction between Na^+ cation and DPA occurs through the triple bond facially coordinated to Na^+ cation near the O atoms binding Al atoms. The shortest distance between Na^+ and C atom of DPA triple bond is 0.24 nm. The same interaction is observed for smaller Li^+ and the shorter distance between cation and C≡C triple bond is 0.22 nm. For larger K^+, Rb^+, Cs^+ cations, the interactions

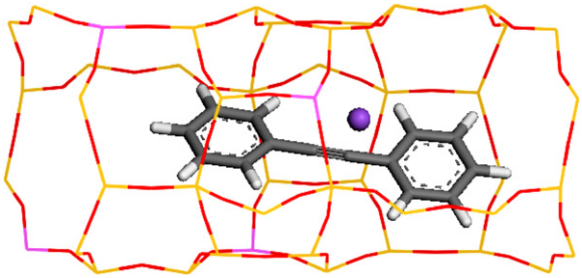

Fig. 3. DPA predicted sorption site in straight channel of NaZSM-5. Red, yellow and pink sticks represent the O, Si and Al atoms of the framework, respectively. The white and shaded cylinders represent the H and C atoms of the DPA ($C_{14}H_{10}$) molecule, respectively. The purple sphere represents the Na^+ cation.

occur through one phenyl group facially coordinated to the cation and the distances between the molecule and the extra framework cation increase progressively with the cation size. The shortest distance between K^+, Rb^+, Cs^+ and the C atom of DPA phenyl ring are 0.30, 0.32, 0.33 nm, respectively. The tight fit of DPA in the pores with bulky cations can reduce the DPA mobility in rigid zeolite pores below the isotropic limit characteristic of a liquid. In such constrained confinement the electrostatic effect can induce new Raman bands typical of the local symmetry.

3.3. Spectroscopic and kinetics studies of species generated by photoionization of DPA occluded in $M_{6.6}$ZSM-5 zeolites

A laser operating at 266 nm was used to irradiate the DPA@silicalite-1 and DPA@$M_{6.6}$ZSM-5 (M = Li^+, Na^+, K^+, Rb^+, Cs^+) samples. To ensure that equilibrium was reached for all samples, photolysis was carried out several months after the mixing of dehydrated zeolites and solid DPA. The photolysis wavelength falls within the contour of the electronic transitions of occluded DPA (Fig. 1). The irradiation of DPA@silicalite-1 sample did not induce any color change and no spectral change was observed using conventional spectroscopic tools. In contrast, the white powder turned light green immediately after the 15 s irradiation period of DPA@$M_{6.6}$ZSM-5 (M = Li^+, Na^+, K^+, Rb^+, Cs^+). This color turned to brownish pink with time. The photoinduced reaction was followed by DRUVv spectroscopy at room temperature over 2 days after the irradiation. Characteristic absorption bands at 378, 401, 418, 495 and 535 nm were observed immediately after laser photolysis of DPA@$Li_{6.6}$ZSM-5 sample. For longer time, only the bands at 495 and 535 nm remain. In contrast, the DRUVv spectra recorded after irradiation of DPA@$M_{6.6}$ZSM-5 (M = Na^+, K^+, Rb^+, Cs^+) exhibit only broad band with two maxima centered at ca. 495 and ca. 538 nm (Fig. 4A–C).

The data processing of the spectral sets was carried out using the MCR approach (see Section 2) to resolve the characteristic spectra of pure species from the mixture generated by photolysis. For irradiated DPA@$Li_{6.6}$ZSM-5 sample, three absorbing species were expected from the matrix rank analysis. As expected, three pure spectra were extracted from the spectral set by the MCR treatment with residuals between experimental and calculated values less than 3%. A resolved spectrum (Fig. 5a) with a prominent band at 298 nm and a shoulder at 284 nm is straightforwardly assigned to DPA occluded as intact molecule in the void space of $Li_{6.6}$ZSM-5 zeolite because of its resemblance with the one band spectrum obtained for DPA occluded within $Li_{6.6}$ZSM-5 before irradiation (Fig. 1). The second spectrum to be resolved shows narrow bands at 378 and 417 nm and a weak broad band at 795 nm (Fig. 5b). This spectrum is assigned to $DPA^{\bullet+}$ because it is identical to the spectrum previously assigned to $DPA^{\bullet+}$ radical cation produced by γ-ray irradiation in frozen matrices [59] and by pulse radiolysis of DPA

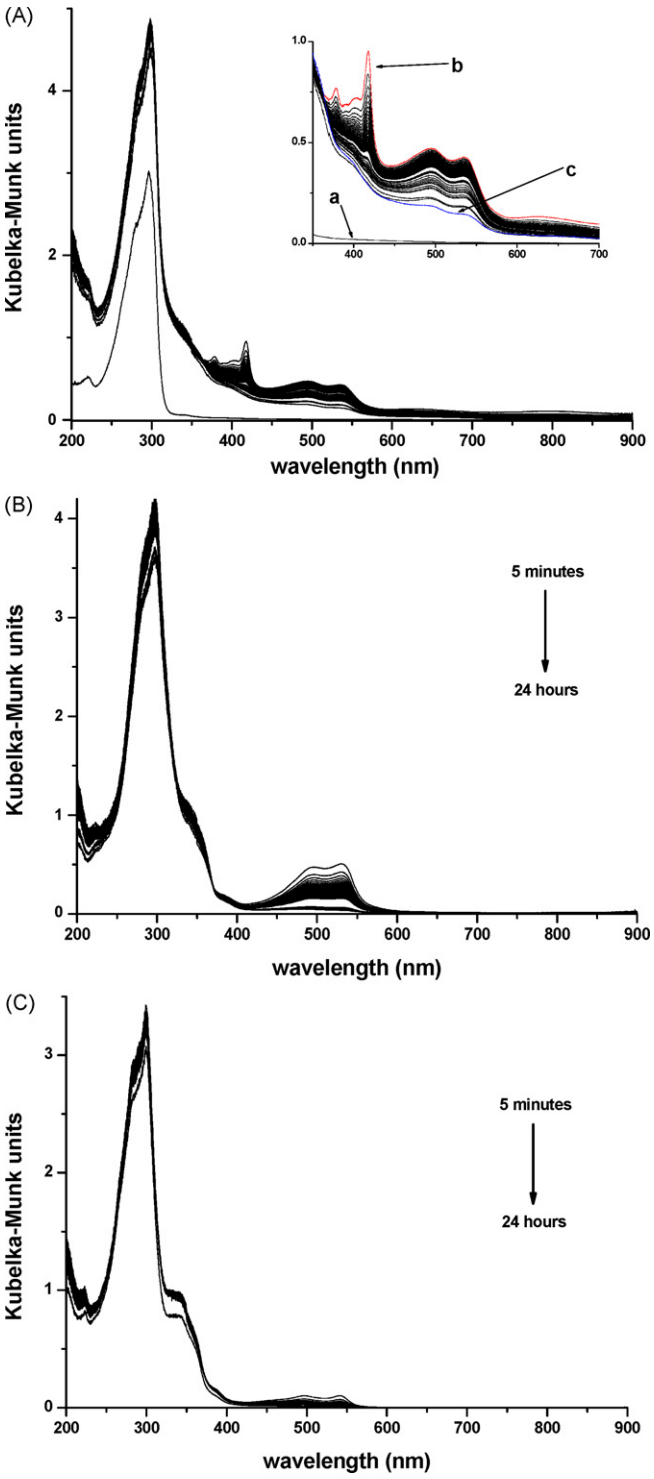

Fig. 4. (A) Diffuse reflectance UV–vis (DRUVv) spectral set recorded after 266 nm laser photolysis of DPA@$Li_{6.6}$ZSM-5 as a function of time. (a) Before photolysis; (b) 5 min after photolysis; (c) 4 days after photolysis. (B) DRUVv spectral set recorded for 24 h after DPA@$K_{6.6}$ZSM-5 photolysis (λ = 266 nm). (C) DRUVv spectral set recorded for 24 h after DPA@$Cs_{6.6}$ZSM-5 photolysis (λ = 266 nm).

in solution [60]. The third extracted spectrum shows a broad band between 400 and 550 nm with two maxima centered at 495 and 535 nm (Fig. 5c). These absorption bands are still observed after the $DPA^{\bullet+}$ spectral signature complete disappearance. Moreover, this absorption looks like the charge transfer band obtained after the photoionization of *t*-stilbene occluded within ZSM-5 zeolites [34]. Analogous spectral features were also previously observed

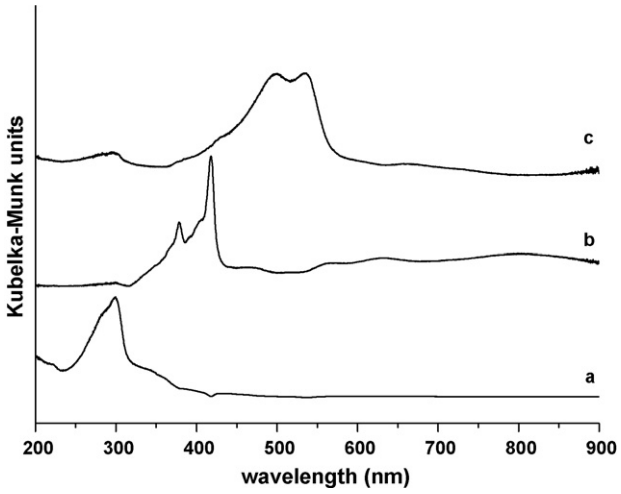

Fig. 5. DRUVv spectra of pure species resolved using multivariate curve resolution (MCR) method from the spectral set recorded after DPA@$Li_{6.6}$ZSM-5 photoionization. (a) DPA@$Li_{6.6}$ZSM-5; (b) DPA$^{\bullet+}$@$Li_{6.6}$ZSM-5$^{\bullet-}$; (c) DPA@$Li_{6.6}$ZSM-5$^{\bullet+\bullet-}$.

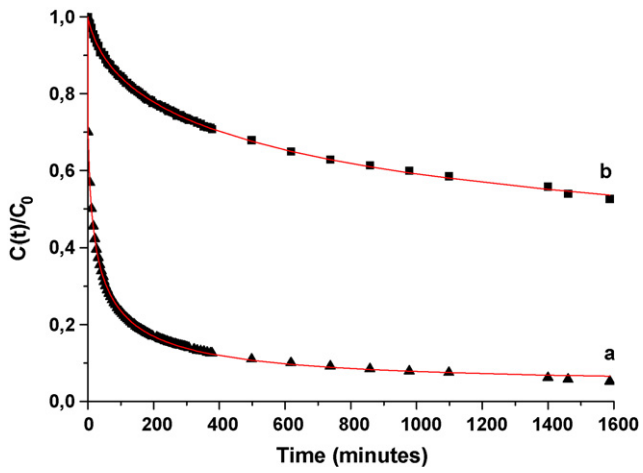

Fig. 6. (a) Decay of $C(t)/C_0$ relative concentration of DPA$^{\bullet+}$@$Li_{6.6}$ZSM-5$^{\bullet-}$ moiety generated by photoionization as a function of time. (b) Decay of DPA@$Li_{6.6}$ZSM-5$^{\bullet-\bullet+}$ electron–hole pair concentration recorded as a function of time. The relative concentrations are obtained by the multivariate curve resolution method and correspond to spectra b and c of Fig. 5, respectively.

after spontaneous and photoionization of biphenyl and naphthalene [32,33]. By comparison with these works this absorption band is assigned to electronic transitions of electron–hole pair trapped in DPA@$Li_{6.6}$ZSM-5. The spectrum features are related to hole transfer from radical cation to zeolite framework after photoionization. It is highly probable that the disappearance of the DPA$^{\bullet+}$ is related to the electron donor ability of ZSM-5 framework towards electron deficient DPA$^{\bullet+}$ rather than direct charge recombination.

The broad absorption band observed in the visible domain is tentatively assigned to an interfacial charge transfer band involving the molecule and hole of zeolite. The whole electron–hole pair is considered as the absorbing moiety in our discussion but so far, the exact nature of the transition has not been established in this case. Nevertheless, we have demonstrated previously that absorption of light within the charge transfer band of electron–stilbene–hole results in interfacial hole transfer from zeolite to sorbate to induce radical cation/electron pair in the excited state [34]. The hole migration by electron hopping between neighbor oxygens was already observed in germanium containing ITQ-17 zeolite. This process led also to a charge separated state that decay by a non-geminate recombination pathway [20].

No spectroscopic evidence of ejected electron of the DPA$^{\bullet+}$-electron moiety was found using the MCR approach. It is likely that the trapped electron spectrum is very weak and broad and not clearly detected in the baseline of the DRUVv spectra. The electron spectral signature was already reported in bare zeolite after pulsed electron radiolysis as Na_4^{3+} cluster [61,62]. The lifetime of these species was found to be in the microsecond timescale. If such moiety was created in the DPA@MZSM-5 system, the short lived transient behavior of these species would prevent their observation by using conventional spectroscopic tools.

After DPA@$M_{6.6}$ZSM-5 irradiation with M = Na^+, K^+, Rb^+, Cs^+, data processing never allow the observation of DPA$^{\bullet+}$ radical cation. The two extracted spectra correspond to occluded DPA and to electron–hole pair as obtained above. Nevertheless, even though radical cation is not observed because of probable too short lifetime, DPA$^{\bullet+}$-electron moiety is assumed to be initially generated by photolysis whatever the extra framework cation. Therefore, the photolysis occurs according to the following reaction:

$$\text{DPA@M}_{6.6}\text{ZSM-5} + h\nu \rightarrow \text{DPA}^{\bullet+}\text{@M}_{6.6}\text{ZSM-5}^{\bullet-} \quad (6)$$

DRUVv values using the Kubelka–Munk scale provide suitable evaluation of intensities proportional to concentrations of the components. Data processing using MCR software of spectral sets resolved pure UV–vis spectra of absorbing species and gave the respective contribution $C(t)$ of each absorbing species as a function of time. Normalization of $C(t)/C_0 = 1$ at $t = 0$ was used to obtain the relative contribution of each component as a function of time.

The curves (a and b) of Fig. 6, exhibit the specific $C(t)/C_0$ decays of DPA$^{\bullet+}$ and electron–hole pair measured after the photolysis of DPA@$Li_{6.6}$ZSM-5, respectively. The decays were accurately simulated according to the Albery kinetic model detailed in Section 2. The best values of $\bar{k}$ average rate constants deduced by fitting are listed in Table 1. The corresponding γ distribution coefficients (see Section 2) range between 2 and 3, in reasonable agreement with other heterogeneous photochemical reactions [63].

The corresponding lifetimes are conventionally represented by $1/\bar{k}$. The values obtained for DPA@$Li_{6.6}$ZSM-5 show that the DPA$^{\bullet+}$ lifetime is shorter than that of electron–hole pair one. The rate of the electron–hole pair formation was not evidenced for DPA@$Li_{6.6}$ZSM-5 but is expected to be correlated to the DPA$^{\bullet+}$ disappearance. The DPA$^{\bullet+}$@$Li_{6.6}$ZSM-5$^{\bullet-}$ charge recombination is assumed to be very slow by comparison with electron abstraction and therefore, electron abstraction from the zeolite framework by DPA$^{\bullet+}$ is assumed to generate long-lived electron–hole pair before total charge recombination:

$$\text{DPA}^{\bullet+}\text{@Li}_{6.6}\text{ZSM-5}^{\bullet-} \rightarrow \text{DPA@Li}_{6.6}\text{ZSM-5}^{\bullet-\bullet+} \quad (7)$$

The size increase of the counterbalancing cation from Li^+ to Cs^+ is expected to increase the basicity of framework oxygen, which is expected to enhance the electron donor properties of the zeolite framework [64]. The DPA@$M_{6.6}$ZSM-5$^{\bullet-\bullet+}$ electron–hole pair concentration decays calculated for M = Na^+, K^+, Rb^+ and Cs^+ are presented in Fig. 7. The disappearance rate was found to be in

Table 1
Kinetic and spectroscopic results of DPA$^{\bullet+}$-electron and electron–hole pair photoinduced by photolysis of DPA@$M_{6.6}$ZSM-5 (λ = 266 nm).

$M_{6.6}$ZSM-5 M	DPA$^{\bullet+}$-electron $\bar{k}$ min^{-1} (γ)	DPA$^{\bullet+}$ λ_{max} (nm)	Electron–hole $\bar{k}$ min^{-1} (γ)	Electron–hole λ_{max} (nm)
Li^+	0.055 (2.8)	379; 418	0.0078 (3.0)	494; 535
Na^+	–		0.0117 (1.5)	495; 540
K^+	–		0.0146 (2.5)	495; 531
Rb^+	–		0.0151 (2.3)	497; 539
Cs^+	–		0.051 (1.9)	497; 540

$\bar{k}$ is the average first order rate constant of the Albery function with corresponding γ (in parentheses) distribution coefficient.

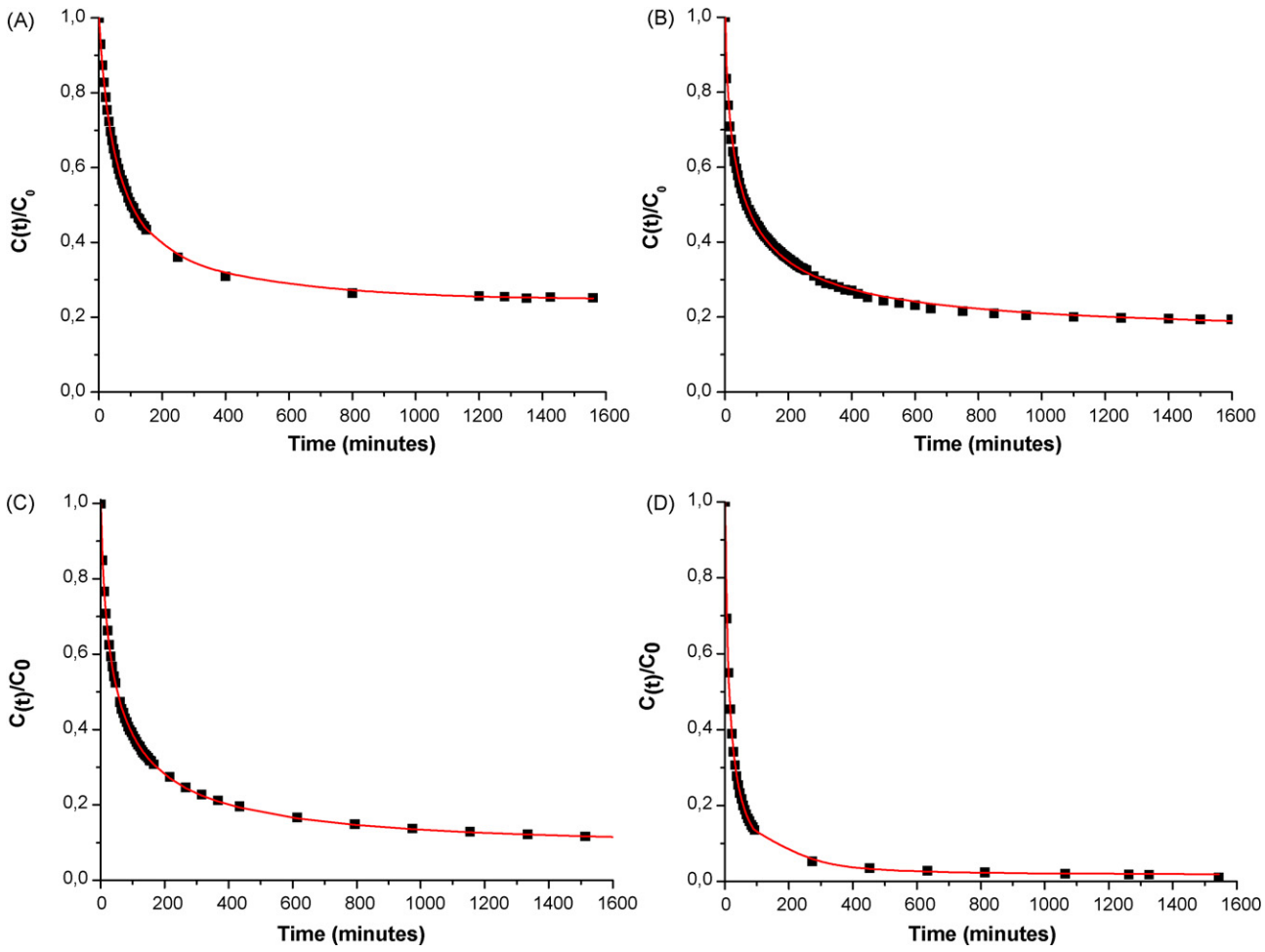

Fig. 7. Decay of DPA@$M_{6.6}$ZSM-5$^{\bullet-\bullet+}$ electron–hole pair concentration recorded as a function of time after DPA@$M_{6.6}$ZSM-5 photoionization. The relative concentration is obtained by the multivariate curve resolution method. (A) M = Na^+; (B) M = K^+; (C) M = Rb^+; (D) M = Cs^+.

close relation with the electron donor properties of the framework but probably involved other parameters. The DPA@$M_{6.6}$ZSM-5$^{\bullet-\bullet+}$ electron–hole recombination rate decreases with the cation nature in the following order: $Cs^+ > Rb^+ \sim K^+ > Na^+ > Li^+$. The charge recombination went to completion according to the following Eq. (8) over less than 1 h for Cs^+ but requires several hours for Li^+:

$$\text{DPA@}M_{6.6}\text{ZSM-5}^{\bullet-\bullet+} \rightarrow \text{DPA@}M_{6.6}\text{ZSM-5} \quad (8)$$

The Raman spectra recorded using the 1064 nm exciting line after DPA@$Li_{6.6}$ZSM-5 photoexcitation immediately and for several hours after the irradiation off are presented in Fig. 8. The spectrum obtained 15 min after photolysis shows clearly the characteristic features of DPA at 997, 1142 and 1593 cm^{-1} but the 1481 cm^{-1} line is not observed. Moreover, new bands are observed at ca. 1100, 1200–1230, 1295, 1316, 1342, 1435, 1515, 1540 and 1615 cm^{-1} (Fig. 8b). The intensity of these new bands decreases progressively with time. After 2 days, the Raman spectrum shows only the 997, 1142, 1481 and 1593 cm^{-1} lines of DPA in agreement with total recombination (Fig. 8f). It is worth noting that upon photolysis, the FT spectra exhibit strong parasite absorptions between 2000 and 2400 cm^{-1}. These bands are due to the absorption of the exciting light by the air molecules and more particularly by the H_2O molecules on the optical path between sample and light source. In the absence of reaction, luminescence does not occur and the observation of the triple bond stretching mode at about 2200 cm^{-1} is possible. However, after photolysis, the DPA photoionization reaction induces huge luminescence and the intensity of the parasite absorption bands increases drastically with the luminescence phenomena. These bands hide totally the 2000–2500 cm^{-1} domain and therefore, the behavior of the triple bond mode during the reaction advancement cannot be studied using FT-Raman spectrometry.

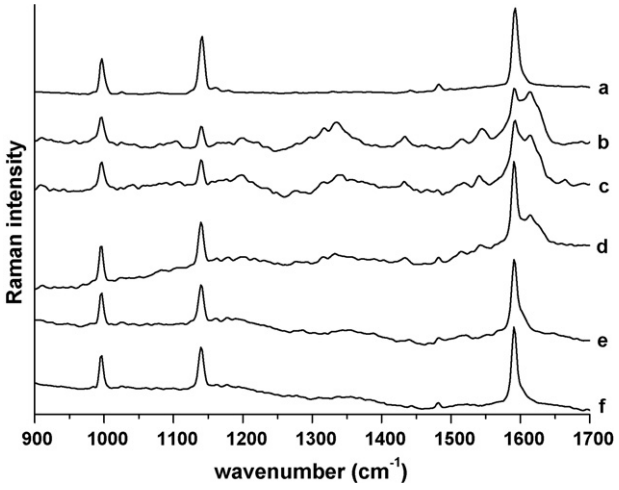

Fig. 8. FT-Raman (λ = 1064 nm) spectra recorded as a function of time after the photolysis of DPA@$Li_{6.6}$ZSM-5. (a) Before photolysis; (b) 15 min after photolysis; (c) 1 h after photolysis; (d) 2 h; (e) 24 h; (f) 2 days after photolysis.

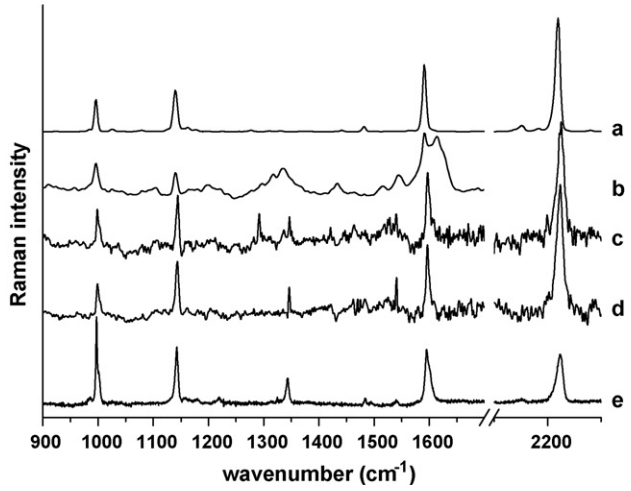

Fig. 9. Raman spectra recorded after the photolysis of DPA@$Li_{6.6}$ZSM-5. (a) Solid DPA; (b) 15 min after photolysis (λ = 1064 nm); (c) 15 min after photolysis (λ = 785 nm); (d) 30 min after photolysis (λ = 785 nm); (e) 15 min after photolysis (λ = 632.8 nm).

The Raman spectra recorded using the 785 nm exciting wavelength after DPA@$Li_{6.6}$ZSM-5 laser irradiation show also new bands centered at 1105, 1292, 1335 and 1345, 1420, 1518 and 1528, 1540, 1610 in addition to the DPA Raman lines at 998, 1144, 1597 and 2223 cm^{-1} (Fig. 9c). After several hours, most of these lines disappear and only the 1341 and the 1540 cm^{-1} line are still clearly observed (Fig. 9d). These lines are no more visible after 3 days.

Using the 632.8 nm excitation line, the spectrum recorded 15 min after DPA@$Li_{6.6}$ZSM-5 photolysis shows mainly the 998, 1142, 1484, 1595 and 2223 cm^{-1} DPA lines and exhibits relative intensity changes with respect to the spectrum recorded with the 785 nm exciting line (Fig. 9e). Nevertheless, an intense band is also observed at 1344 cm^{-1}. This line was already observed using the 785 and 1064 nm excitation lines. Furthermore, weak bands at 1220, 1540 cm^{-1} and ca. 1605 cm^{-1} as a shoulder of the 1595 cm^{-1} line are also observed.

Whatever the exciting wavelength, the Raman spectra recorded after photolysis never exhibit the Raman features of $DPA^{\bullet+}$ and so far, the observed Raman patterns were never reported. Nevertheless, in comparison with previous results obtained with *t*-stilbene and other polyaromatics, the unknown prominent lines are assigned to internal normal modes of the DPA@$Li_{6.6}$ZSM-$5^{\bullet-\bullet+}$ moiety at the ground state [34]. The frequency shifts and relative intensity changes with respect to the DPA@$Li_{6.6}$ZSM-5 spectrum are probably induced by the electrostatic field of the surrounding charges. The $DPA^{\bullet+}$ concentration is probably too weak to be detected without resonance effect. This behavior is in agreement with the charge recombination of electron–hole pair as shown by using DRUVv spectrometry.

4. Discussion

Diffuse reflectance UV–vis absorption and Raman scattering data obtained during the sorption of DPA in Al-free silicalite-1 and in Al-rich $M_{6.6}$ZSM-5 provide evidence of neutral DPA occluded in the void space of ZSM-5 after several weeks of exposure of solid DPA to empty zeolite at room temperature. However, the organization period is very slow and depends on the charge balancing cation size. Molecular modeling demonstrates that silicalite-1 and $M_{6.6}$ZSM-5 straight channel openings are sufficiently wide to allow DPA molecule to enter through them and to slowly diffuse into the porous void space. DPA lies in the straight channel at the intersection with the sinusoidal channel in interaction with the extraframework cation. Within $M_{6.6}$ZSM-5, DPA is in the close proximity of M^+ and Al atom of the framework. Moreover, it is likely that larger extra framework cations such as K^+, Rb^+ or Cs^+ slow down the DPA mobility in the channel and promote the breakdown of the D_{2h} molecular symmetry as shown by Raman spectroscopy.

It is worth noting that within silicalite-1 and $M_{6.6}$ZSM-5, the intrazeolithe electrostatic field gradient is too weak to induce DPA (I_p = 7.94 V) spontaneous ionization even with the rather high polarizing Li^+ cation.

The photolysis of DPA occluded within silicalite-1 did not show any photoinduced ionization on the studied time scale. Possible reaction of ionization would require the application of time resolved optical absorption spectroscopy to be evidenced. In contrast, the laser excitation of DPA adsorbed in $Li_{6.6}$ZSM-5 generates long-lived radical cation and subsequent electron–hole pair. The fate of these moieties was monitored successfully by conventional spectroscopic techniques over several days. The spectroscopic and kinetic results obtained during the DRUVv investigations point out the $DPA^{\bullet+}$-electron moiety formation in $Li_{6.6}$ZSM-5 and subsequent electron transfer to persistent electron–hole pair before the charge recombination. This primary reaction of ionization is a fast phenomenon and is only observed in $Li_{6.6}$ZSM-5. Within $M_{6.6}$ZSM-5 ($M = Na^+$, K^+, Rb^+, Cs^+), the radical cation-electron pair was never observed because of probable ultrafast kinetic but is assumed to be a prerequisite necessary for electron–hole pair formation. The $DPA^{\bullet+}$ disappearance comes from the oxidizing power of $DPA^{\bullet+}$ with respect to electron donor ability of $M_{6.6}$ZSM-5 framework. $DPA^{\bullet+}$ is assumed to capture one other electron from $M_{6.6}$ZSM-5 inner surface to generate long-lived electron–hole pair before the final charge recombination. The electron abstraction or hole transfer rate is faster than the direct $DPA^{\bullet+}$-electron recombination. The DRUVv spectrum assigned to the long-lived DPA@$M_{6.6}$ZSM-$5^{\bullet-\bullet+}$ electron–hole pair exhibits broad bands between 450 and 550 nm. Analogous broad bands were previously observed for long-lived electron–hole pairs generated by photoionization of biphenyl, naphthalene, *t*-stilbene occluded in non-acidic M_nZSM-5 [32–34]. Although these absorption bands are very similar in term of shape, they do not appear exactly at the same wavelength for all the studied molecules. Nevertheless, the energy levels involved in the electronic transition are assumed to be identical and therefore there is nothing surprising about the striking similarities observed for all these molecules. Furthermore, the examination of the electron–hole pair spectra obtained for DPA as well as for biphenyl, naphthalene and *t*-stilbene provides evidence of analogous vibrational progressions with about 1500–1700 cm^{-1} distance between the two main bands. This value undoubtedly involves vibration of the neutral molecule at the excited state and demonstrates the involvement of the molecule in the electron–hole moiety.

Moreover, the Raman spectra of the electron–hole pair obtained by using the 632.8, 785 and 1064 nm exciting lines present specific patterns that were unknown so far. The frequency shifts and relative intensity changes with respect to the DPA@$M_{6.6}$ZSM-5 spectrum are probably induced by the electrostatic field of the surrounding charges. After several days, the Raman spectra display only the characteristic lines of the neutral DPA occluded in $M_{6.6}$ZSM-5.

For identical Si/Al ratio, the electron donor ability of oxygen framework increases with larger alkali metal cations. Therefore, the $DPA^{\bullet+}$@$M_{6.6}$ZSM-$5^{\bullet-}$ ($M = Li^+$, Na^+, K^+, Rb^+, Cs^+) moiety lifetimes should increase in the following order: $Cs^+ < Rb^+ < K^+ < Na^+ < Li^+$. This is in agreement with the longer lifetime observed for $DPA^{\bullet+}$@$Li_{6.6}$ZSM-$5^{\bullet-}$. However, due to the too short $DPA^{\bullet+}$ lifetimes for other cations this assumption cannot be checked properly. The persistent DPA@$M_{6.6}$ZSM-$5^{\bullet-\bullet+}$ electron–hole pairs disappear after several hours through charge recombination. The electron–hole

recombination depends on M^+ and appears to be also in relation with the electron donor properties of the framework. The charge recombination rate decreases in the order $Cs^+ > Rb^+ \sim K^+ > Na^+ > Li^+$.

The stabilization of $DPA^{\bullet+}$-electron pair and $DPA@M_{6.6}ZSM\text{-}5^{\bullet-\bullet+}$ electron–hole pair depend on the combined effects of confinement which dramatically reduces the DPA mobility in the zeolite void space and can promote the breakdown of the D_{2h} molecular symmetry and on the intrazeolithe electrostatic field of $DPA@M_nZSM\text{-}5$ ($M = Li^+$, Na^+, K^+, Rb^+, Cs^+). Moreover, forces that drive transport in zeolite include concentration gradient and electric potential gradient. The radical cation and electron are created by photoionization and the resulting species diffuse across the porous void at different rates. This phenomenon is known as the compartmentalization of charges [18].

For Li^+, Na^+, K^+ Rb^+, Cs^+ charge compensating cations, the bond is largely ionic and the mean electric field is supposed to be large. Nevertheless, the electrostatic field gradient depends also drastically and principally on the van der Waals radius of the extraframework cations. Therefore, the very short radius of Li^+ induces high local gradient electrostatic field and therefore higher stabilization. Note that ionization depends also on the ionization potential of the occluded molecule. The electron and radical ion as well as the electron–hole pair do not move independently but create a charge imbalance.

Charge recombination depends on the reaction free energy ΔG^0 that is <0. According to non-adiabatic electron transfer theory the driving force dependence on the hole transfer rate can be given by the following equation:

$$\text{electron transfer rate} = \left[\frac{4\pi^3}{(h^2\lambda k_B T)}\right]^{-1/2} |H|^2 \times \exp\left[\frac{-(\Delta G^0 + \lambda)^2}{(4\lambda k_B T)}\right] \quad (9)$$

where H is the electronic coupling between the donor and acceptor states, ΔG^0 is the reaction free energy and λ is the reorganization energy [65]. The term H^2 corresponds to electron tunneling through a potential barrier and therefore shows an exponential dependence upon spatial separation r of the donor and acceptor states:

$$H^2 = H_0^2 \exp[-\beta r] \quad (10)$$

where β is a function of the barrier height. It is apparent from this equation that the internal surface topology of zeolite pores can modulate the electron transfer dynamics by varying the H^2, ΔG^0, and λ values. The value of reorganization energy (λ) was reported to be small in rigid framework and is largely controlled by the tight fit between sorbate size and pore dimensions [66].

ΔG^0 corresponds to the difference in free energy between the DPA oxidation midpoint potential (E_0) and the highest occupied valence band energy of $M_{6.6}ZSM\text{-}5$. Unfortunately, there is no direct information about this energy level. The small reorganization energy (λ) coupled with large negative free energy changes ($-\Delta G^0$) might explain the slow recombination of photoinduced charge separated state. The large distance between unpaired electrons which occurs after ionization upon photolysis in $M_{6.6}ZSM\text{-}5$ can be invoked to explain the very slow charge recombination.

References

[1] W. Hu, H. Nakashima, K. Furukawa, Y. Kashimura, K. Ajito, Y. Liu, D. Zhu, K. Torimitsu, J. Am. Chem. Soc. 127 (2005) 2804–2805.
[2] M.A. Reed, J. Chen, A.M. Rawlett, D.W. Price, J.M. Tour, Appl. Phys. Lett. 78 (2001) 3735–3737.
[3] C. Li, D. Zhang, X. Liu, S. Han, T. Tang, C. Zhou, W. Fan, J. Koehne, J. Han, M. Meyyappan, A.M. Rawlett, D.W. Price, J.M. Tour, Appl. Phys. Lett. 82 (2003) 645–647.
[4] J.M. Tour, M. Kozaki, J.M. Seminario, J. Am. Chem. Soc. 120 (1998) 8486–8493.
[5] C. Hortholary, C. Coudret, J. Org. Chem. 68 (2003) 2167–2174.
[6] D.J. Dyer, V.Y. Lee, R.J. Twieg, Liq. Cryst. 24 (1998) 271–281.
[7] Y. Hirata, T. Okada, T. Nomoto, J. Phys. Chem. A 102 (1998) 6585–6589.
[8] A.C. Benniston, A. Harriman, J.P. Rostron, Phys. Chem. Chem. Phys. 7 (2005) 3041–3047.
[9] T. Takada, K. Kawai, M. Fujitsuka, T. Majima, Angew. Chem. Int. Ed. 45 (2006) 120–122.
[10] F.D. Lewis, X. Liu, S.E. Miller, M.R. Wasielewski, J. Am. Chem. Soc. 121 (1999) 9746–9747.
[11] F.D. Lewis, X. Liu, S.E. Miller, R.T. Hayes, M.R. Wasielewski, J. Am. Chem. Soc. 124 (2002) 14020–14026.
[12] V. Ramamurthy, P. Lakshminarasimhan, C.P. Grey, L.J. Johnson, Chem. Commun. (1998) 2411–2424.
[13] H. Garcia, H.D. Roth, Chem. Rev. 102 (2002) 3947–4007.
[14] A. Corma, H. Garcia, Chem. Rev. 102 (2002) 3837–3892.
[15] T.M. Leu, E. Roduner, J. Catal. 228 (2004) 397–404.
[16] S. Marquis, A. Moissette, H. Vezin, C. Bremard, C. R. Chim. 8 (2005) 419–440.
[17] S. Marquis, A. Moissette, H. Vezin, C. Bremard, J. Phys. Chem. B 109 (2005) 3723–3726.
[18] A.E. Keirstead, N.P. Schepp, F.L. Cozens, J. Phys. Chem. C 111 (2007) 14247–14252.
[19] J.P. Herance, P. Concepcion, A. Domenech, J.L. Bourdelande, J. Marquet, H. Garcia, Chem. Eur. J. 11 (2005) 6491–6502.
[20] M. Alvaro, P. Atienzar, A. Corma, B. Ferrer, H. Garcia, M.T. Navarro, J. Phys. Chem. B 109 (2005) 3696–3700.
[21] P. Atienzar, A. Corma, H. Garcia, J.C. Scaiano, Chem. Mater. 16 (2004) 982–987.
[22] A. Moissette, S. Marquis, I. Gener, C. Bremard, Phys. Chem. Chem. Phys. 4 (2002) 5690–5696.
[23] A. Moissette, H. Vezin, I. Gener, C. Bremard, J. Phys. Chem. B 107 (2003) 8935–8945.
[24] H. Vezin, A. Moissette, C. Bremard, Angew. Chem. Int. Ed. 42 (2003) 5587–5591.
[25] H. Vezin, A. Moissette, M. Hureau, C. Bremard, ChemPhysChem 7 (2006) 2474–2477.
[26] S. Marquis, A. Moissette, M. Hureau, H. Vezin, C. Bremard, J. Phys. Chem. C 111 (2007) 17346–17356.
[27] J.C. Scaiano, H. Garcia, Acc. Chem. Res. 32 (1999) 783–793.
[28] M. Alvaro, H. Garcia, S. Garcia, F. Marquez, J.C. Scaiano, J. Phys. Chem. 101 (1997) 3043–3051.
[29] S.J. Hashimoto, J. Chem. Soc., Faraday Trans. 93 (1997) 4401–4408.
[30] M.A. O'Neill, F.L. Cozens, N.P. Schepp, J. Phys. Chem. B 105 (2001) 12746–12758.
[31] K.T. Ranjit, L. Kevan, J. Phys. Chem. B 106 (2002) 1104–1109.
[32] I. Gener, A. Moissette, C. Bremard, Phys. Chem. Chem. Phys. 6 (2004) 3732–3738.
[33] A. Moissette, S. Marquis, D. Cornu, H. Vezin, C. Bremard, J. Am. Chem. Soc. 127 (2005) 15417–15428.
[34] A. Moissette, C. Bremard, M. Hureau, H. Vezin, J. Phys. Chem. C 111 (2007) 2310–2317.
[35] S. Marquis, A. Moissette, C. Bremard, ChemPhysChem 7 (2006) 1525–1534.
[36] C. Bremard, M. Lemaire, J. Phys. Chem. 97 (1993) 9695–9702.
[37] E. Beerdsen, D. Dubbeldam, B. Smit, T.J.H. Vlugt, S. Calero, J. Phys. Chem. B 107 (2003) 12088–12096.
[38] B.F. Mentzen, J. Phys. Chem. C 111 (2007) 18932–18941.
[39] B.F. Mentzen, G.U. Rakhmatkariev, G. Bergeret, H.-P. Weber, J. Phys. Chem. C 111 (2007) 3820–3830.
[40] D.H. Olson, N. Khosrovani, A.W. Peters, B.H. Toby, J. Phys. Chem. B 104 (2000) 4844–4848.
[41] B.F. Mentzen, G. Bergeret, H. Emerich, H.-P. Weber, J. Phys. Chem. B 110 (2006) 97–106.
[42] B.F. Mentzen, G. Bergeret, H. Emerich, H.-P. Weber, J. Phys. Chem. B 110 (2006) 13741–13752.
[43] C. Morin, D. Simon, P. Sautet, J. Phys. Chem. B 108 (2004) 12084–12091.
[44] C. Baehtz, H. Fuess, Phys. Chem. Chem. Phys. 4 (2002) 4543–4548.
[45] K.B. Wiberg, J. Org. Chem. 62 (1997) 5720–5727.
[46] I. Gener, G. Buntinx, C. Bremard, Micropor. Mesopor. Mater. 41 (2000) 253–268.
[47] W. Windig, B. Antalek, J.L. Lippert, Y. Batonneau, C. Bremard, Anal. Chem. 74 (2002) 1371–1379.
[48] W.J. Albery, P.N. Bartlett, C.P. Wilde, J.R. Darwent, J. Am. Chem. Soc. 107 (1985) 1854–1858.
[49] Z. Chernia, T. Livneh, I. Pri-Bar, J.E. Koresh, Vib. Spectrosc. 25 (2001) 119–131.
[50] A. Shimojima, H. Takahashi, J. Phys. Chem. 97 (1993) 9103–9112.
[51] H. Hiura, H. Takahashi, J. Phys. Chem. 96 (1992) 8909–8915.
[52] H. Susuki, Bull. Chem. Soc. Jpn. 33 (1960) 944–952.
[53] H. Van Koningsveld, J.C. Jansen, H. Van Bekkum, Zeolites 10 (1990) 235–242.
[54] H. Van Koningsveld, Acta Crystallogr. B46 (1990) 731–735.
[55] H. Van Koningsveld, J.C. Jansen, H. Van Bekkum, Zeolites 7 (1987) 564–568.
[56] A. Borodin, M. Yamazaki, N. Kishimoto, K. Ohno, J. Phys. Chem. A 110 (2006) 1783–1790.
[57] D. Xu, A.L. Cooksy, J. Mol. Struct.: Theochem 815 (2007) 119–125.
[58] Y. Li, J. Zhao, X. Yin, H. Liu, G. Yin, Phys. Chem. Chem. Phys. 9 (2007) 1186–1193.
[59] H. Susuki, K. Koyano, T. Shida, A. Kira, Bull. Chem. Soc. Jpn. 55 (1982) 3690–3701.
[60] S. Yamamoto, Y. Yamamoto, K. Hayashi, Bull. Chem. Soc. Jpn. 64 (1991) 346–351.

[61] N.P. Blake, V.I. Srdanov, G.D. Stuky, H. Metiu, J. Phys. Chem. 99 (1995) 2127–2133.
[62] X. Liu, G. Zhang, J.K. Thomas, J. Phys. Chem. 99 (1995) 10024–10034.
[63] I. Gener, G. Buntinx, A. Moissette, C. Bremard, J. Phys. Chem. B 106 (2002) 10322–10329.
[64] S.J. Hashimoto, J. Photochem. Photobiol. C: Photochem. Rev. 4 (2003) 19–49.
[65] R.A. Marcus, N. Sutin, Biochim. Biophys. Acta 811 (1985) 265–322.
[66] K.G. Thomas, V. Biju, P.V. Kamat, M.V. George, ChemPhysChem 4 (2003) 1299–1307.